A.T. Conn et al., Int. J. of Design & Nature and Ecodynamics. Vol. 3, No. 1 (2008) 12–27

THE DESIGN OPTIMISATION OF AN INSECT-INSPIRED MICRO AIR VEHICLE

A.T. CONN, S.C. BURGESS, C.S. LING & R. VAIDYANATHAN
Department of Mechanical Engineering, University of Bristol, UK.

ABSTRACT

Insect-inspired micro air vehicles (MAVs) have been the subject of extensive research in recent years for a range of novel applications. The current generation of vehicles, however, has yet to match even a fraction of the performance of insect flight, in particular with respect to manoeuvrability and payload capacity. Precise reproduction of insect-like flapping motion on the micro-vehicle scale holds significant potential to address this deficiency. The design and optimisation of this critical aspect of an insect-inspired MAV is the subject of this paper. The actuated flapping mechanism must deliver a high power output via complex wing kinematics, which should be dynamically adjustable for controlled flight without the need for traditional control surfaces. This paper first addresses several key flapping MAV design criteria that greatly influence the power requirements and aerodynamic forces for flight, through an assessment of design parameters such as wing length and wingbeat frequency. Two solutions are then proposed that meet these requirements while satisfying the current limitations of miniature actuation technologies and issues related to mechanism constraint. The first of these, the development of an 'artificial muscle' actuator is crucial to the feasibility of a highly adjustable, lightweight under-constrained flapping mechanism. A prototype 'artificial muscle' based on a silicone dielectric elastomer was tested and found to produce a strain output comparable to muscle. We also report the development of an alternative flapping mechanism solution utilising conventional rotary DC motors. The novel parallel crank-rocker (PCR) mechanism produces similar wing kinematics to insects and, unlike previously developed DC motor-driven MAV flapping mechanisms, it allows dynamically adjustable control of the wing angle of attack. Aerodynamic testing of a PCR prototype found that it produced a maximum lift force of 6.4 g per wing pair at a wingbeat frequency of 13.2 Hz. Wind tunnel testing with high-speed flow visualisation footage showed that the measured lift forces are augmented by a bound leading edge vortex on the downstroke, which is the most important unsteady aerodynamic phenomenon attributed to insect flight.

Keywords: artificial muscle, dielectric elastomer, electro-active polymer, flapping mechanism, insect flight, micro air vehicle, parallel crank-rocker.

1 INTRODUCTION

Extracting functional, structural or aesthetical features from biological systems has the potential to provide operational solutions that outperform designs based on standard engineering practice. This paradigm applies equally to micro air vehicles (MAVs), a class of aircraft defined as having a maximum dimension fewer than 15 cm that operate at speeds under 25 mph [1]. Controllable MAV flight through confined, indoor environments opens an unprecedented breadth of defence and civilian applications, but also demands great agility, controllability, and the capacity to hover. While conventional flight platforms that utilise fixed wing, flexible wing, rotary wing and lighter-than-air designs each have certain advantages, none has demonstrated the capacity for highly manoeuvrable indoor flight at MAV scale [2]. Agile indoor flight is, therefore, a daunting engineering challenge, yet insects, aided by non-orthogonal flight forces and unsteady aerodynamic phenomena, regularly display remarkable flight performance that eclipses these criteria.

The discovery and continuously improving understanding of the low Reynolds number unsteady aerodynamic mechanisms employed by insects is central to applying biomimetic or bio-inspired design to extract flapping wing MAV solutions. Reproducing these designs, hence enabling characteristics of their advanced performance, is a promising approach to allow flapping MAVs to generate greater lift and manoeuvrability than conventional mechanisms for indoor flight, such as rotary wings.

ISSN: 1755-7437 (paper format), ISSN: 1755-7445 (online), http://journals.witpress.com
DOI: 10.2495/D&NE-V3-N1-12-27

Furthermore, common to most complex biological systems, elucidation of insect design parameters offers the concomitant benefit of conferring a wealth of additional information that may be beneficial to other aspects of MAV design. For example, the optic flow method of obstacle avoidance has been successfully utilised in MAVs [3] and *campaniform sensillum*, an insect mechanoreceptor, has been replicated to form novel miniature strain sensors by Skordos *et al.* [4].

The converse trade-off in design inspired by complex biological systems, however, must involve acknowledgment of the inherent limitations of existing technologies. Biological inspiration offers a wealth of promise, yet many synthetic materials are not at a state of maturity where they may be effectively implemented on small autonomous vehicles. Issues related to reproducing the complex insect flight system have led some researchers to develop flapping MAVs that only partially mimic insects, by employing mechanically simplified flapping kinematics coupled with conventional control surfaces such as rudders and ailerons [5–7]. Despite some of these flapping MAVs having the capacity for hovering, none comes close to the manoeuvrability of insects. Paramount among their limitations is that the stabilising and manoeuvring forces produced by their control surfaces are proportional to the *flight* velocity squared, unlike insect wings where the control forces are proportional to the *flapping* velocity squared. The current generation of MAVs is yet to achieve even a fraction of the performance and flexibility of insect flight.

In this paper, the technological difficulties involved in replicating insect flight with a MAV will be addressed and two solutions will be demonstrated. After presenting a brief analysis of insect flight in Section 2 and estimates of the power requirements for flapping MAVs in Section 3, it will be shown in Section 4 that there is a lack of linear output actuation technologies that can replicate the performance of biological muscle at a MAV scale. This has led to the adoption of constrained flapping mechanisms driven by rotary output actuators by other researchers, so two alternative solutions are proposed in Section 5. The first, described in Section 6, involves the development of an emergent actuation technology, dielectric elastomers, that have the potential to match the performance characteristics of muscle. The second solution described in Section 7 is a novel flapping mechanism which, unlike all previously developed rotary motor driven MAV flapping mechanisms, produces wing kinematics that are dynamically adjustable.

2 INSECT FLIGHT

The key feature of insect flight that a flapping MAV should replicate is the variety of unsteady aerodynamic phenomena that greatly augment the lift forces produced. The four main unsteady aerodynamic mechanisms that have been observed in insect flight are the leading edge vortex (LEV) with dynamic stall [8], rotational forces [9], wake recapture [10] and clap and fling [11]. The theory behind these mechanisms is reviewed by Sane [12] and Lehmann [13]. Reproducing some or all of these aerodynamic mechanisms does not necessarily require insect wing kinematics to be similarly mimicked, e.g. the MAV developed by Michelson [14] produces stable LEVs from simplified wing kinematics. However, the ultimate aim of replicating the manoeuvrability of insects is best approached by matching the relatively complex wing motion seen in nature. A survey of the values of kinematics parameters that describe the insect wing motion for suitable species can be found in Conn *et al.* [15].

While replicating the values of the wing kinematic parameters provides a design starting point for reproducing the unsteady aerodynamic mechanisms, it is perhaps more important to also replicate the *adjustment* of these parameters that insects employ for controlled, manoeuvrable flight. Insects adjust various kinematic parameters for flight control, with the high number of control inputs they possess suggesting the use of beneficial control redundancy [16]. The most important of these parameters, which also influences LEVs and unsteady rotational forces, is the wing angle of attack during both the translatory mid-stroke and the timing of pronation and supination relative to stroke

reversal [15]. Beyond the kinematics and aerodynamics of insect flight, the flight apparatus and musculature possesses a wealth of beneficial biomimetic features, which are beyond the scope of this paper to list. Perhaps the most notable physiological feature is the combined use of elastic storage and resonant operation. This greatly reduces the energy expenditure due to accelerating the wing inertia and has significant benefits for a flapping MAV.

3 POWER REQUIREMENTS FOR MAV FLIGHT

In order to design the actuated flapping mechanism and accurately evaluate the many available actuator technologies, whose relative performance characteristics vary greatly, it is essential to perform power requirement analysis for flapping flight. In this section a process of optimising the major design parameters will be presented to estimate the power requirements and hence generate benchmarks for actuator performance.

3.1 Aerodynamic power

From Ellington [17], the mean lift, $\overline{L}$ (in newtons) generated by a pair of flapping wings during hovering can be estimated by:

$$\overline{L} = 3.796 \frac{\Phi^2 n^2 R^4 \overline{C}_L}{AR} \tag{1}$$

where Φ is the stroke amplitude (rad), n is the wingbeat frequency (Hz), R is the wing length (m), $\overline{C}_L$ is the mean lift coefficient and AR is the aspect ratio. From eqn (1), $\overline{L}$ and therefore the maximum supportable weight can be seen to be proportional to kinematical parameters $n^2\Phi^2$ and geometrical parameters R^4AR^{-1}. For the wing geometry parameters, lift is proportional to R^4AR^{-1}, which indicates that the wing span should be maximised up to the 15 cm MAV dimensional limit. Since $\overline{L} \propto n^2R^4$, this also suggests that to support a given weight, R should be increased in favour of n [17].

The limited amount of mechanical power that can be generated by miniature actuators means that it is important to assess the power requirements of flight. A useful metric for flapping MAV design can be found by combining the aerodynamic power with eqn (1) to estimate the power per unit of lift. This was demonstrated by Ellington [17], who derived equations for the mass-specific induced power, $\overline{P}^*_{\text{ind}}$, and mass-specific profile power, $\overline{P}^*_{\text{pro}}$ (the parasitic power is zero during hovering):

$$\overline{P}^*_{\text{ind}} = 14.0nR\left(\frac{\Phi \cdot \overline{C}_L}{AR}\right)^{0.5} \tag{2}$$

$$\overline{P}^*_{\text{pro}} = 18.2\Phi nR\left(\frac{\overline{C}_{D,\text{pro}}}{\overline{C}_L}\right) \tag{3}$$

and mass-specific aerodynamic power, $\overline{P}^*_{\text{aero}}$, is the sum of eqns (2) and (3):

$$\overline{P}^*_{\text{aero}} = \overline{P}^*_{\text{ind}} + \overline{P}^*_{\text{pro}} \tag{4}$$

where $\overline{C}_{D,\text{pro}}$ is the mean profile drag coefficient and mass-specific power has the units of W/kg. From eqns (2) and (3), the key parameters for minimising the total mass-specific aerodynamic power, $\overline{P}^*_{\text{aero}}$, are n and R since AR and Φ have a limited range of values, the latter up to 180°. Although $\overline{P}^*_{\text{aero}}$ is similarly proportional to n and R, less power is required if R is increased in favour of n. This is

because $\overline{L}$ varies with n^2R^4 and so a smaller increase in R is required to support a certain mass [17]. The downside of increasing R is a reduced maximum forward flight speed, U, as n has a much greater magnitude than R and the advance ratio, J, is typically kept constant for a certain flight speed. The advance ratio, J, is effectively the ratio of flight speed to the wing velocity [18]:

$$J = \frac{U}{2\Phi nR} \tag{5}$$

From inspecting eqn (5), U is directly proportional to nR provided J is kept constant. Therefore, if a specific mass is be supported (so $\overline{P}_{\text{aero}}$ becomes proportional to nR) and the energy, E, that can be stored within the MAV is fixed, the maximum distance the MAV can fly, x, is independent of n and R (assuming the inertial power expenditure is negligible). This is shown by eqns (6) and (7):

$$t = \frac{x}{U} = \frac{E}{\overline{P}_{\text{aero}}} \tag{6}$$

re-arranging into eqn (7),

$$x = \frac{U}{\overline{P}_{\text{aero}}} E \tag{7}$$

The fact that for a specific mass the range of an MAV is potentially independent of nR, again strongly supports the notion that R should be increased in favour of n.

3.2 Inertial power

Ideally, the actuated flapping mechanism driving a MAV should be mechanically resonant like the insect pterothorax. In practice, previously developed flapping MAVs have required significant inertial power contributions to accelerate the wing mass and virtual mass at the start of each half-stroke. The inertial power requirement to pitch the wing about its longitudinal axis is typically much lower and can thus be neglected, except for very low AR value wings [19]. By assuming that no negative work is required to decelerate the wing during stroke reversal, the mean inertial power can be estimated from the kinetic energy gained while the wing accelerates over the first half of the downstroke or upstroke [20]. Assuming simple harmonic motion for the stroke kinematics, the mean inertial power over the wing stroke is given by eqn (8):

$$\overline{P}_{\text{acc}} = I_{\text{w+v}} \pi^2 \Phi^2 n^3 \tag{8}$$

where $I_{\text{w+v}}$ is the combined moments of inertia of the wing pair, I_{w}, and associated virtual mass, I_{v}. The wing geometry will be simplified here to a rectangular shape with uniform density, ρ_{w}, and equivalent dimensions of length R, chord $\overline{c}$ and thickness $\overline{h}$. The virtual mass per wing, $m_{\text{v}}/2$, can also be approximated to the mass of air in a cylinder with diameter $\overline{c}$ and length R [20]. Therefore, I_{w} and I_{v} for a pair of rectangular wings with mass, m_{w}, can be given by eqns (9) and (10):

$$I_{\text{w}} = 1/3 \cdot m_{\text{w}} R^2 = 2/3 \cdot \rho_{\text{w}} \overline{h}\overline{c} R^3 \tag{9}$$

$$I_{\text{v}} = 1/3 \cdot m_{\text{v}} R^2 = 1/6 \cdot \pi \rho_{\text{air}} \overline{c}^2 R^3 \tag{10}$$

Substituting eqns (9) and (10) into eqn (8) and dividing by eqn (1), once adjusted from N to kg, gives the mass-specific inertial power, $\overline{P}^*_{\text{acc}}$ (W/kg):

$$\overline{P}^*_{\text{acc}} = 1.723\frac{\pi^2 n}{C_L}\left(2\rho_{\text{w}}\overline{h} + \frac{\pi\rho_{\text{air}}R}{AR}\right) \tag{11}$$

where $\overline{c}$ is replaced with $2R/AR$. Equation (11) suggests that $\overline{P}^*_{\text{acc}}$ is proportional to n, since the virtual mass term, which features R, is likely to be negligible. Therefore, maximising the wing length, R, to reduce n will minimise the power required to overcome inertia.

3.3 Estimate of power expenditure

Equations (4) and (11) will now be used to estimate the power expenditure for hovering flight. Since power expenditure is dependent on numerous variables that can vary greatly, the focus here will be on an MAV with a total mass of 12 g. It will be assumed that Φ is equal to 100°, AR is equal to 7 and the wings have a sectional mass of 0.05 g/cm. As mentioned previously, to support a known mass it is more efficient to maximise R and reduce n, with the negative effect of reducing the maximum flight speed. Therefore, the energetic cost of maximising the flight speed for the 12 g MAV will be considered. Based on the maximum dimensional limit for MAVs of 15 cm, *MAV A* has a wing length of 75 mm, therefore to support 12 g, n must be at least 33.6 Hz. Conversely, *MAV B* has an arbitrary value of n = 75 Hz meaning R has to be at least 50.2 mm. These values of n and R can be used to estimate the maximum flight speed, U_{max}, using eqn (5). Assuming a maximum value of J of one, the maximum flight speed of MAV A is 8.8 m/s while for the shorter-winged MAV B it is 13.1 m/s. A final design parameter to consider is the elastic storage efficiency, η_{elastic}, of kinetic (inertial) energy. Elastic storage efficiency is introduced to assess how it affects both the overall power expenditure and the dynamic efficiency, η_{dyn}, given by eqn (12):

$$\eta_{\text{dyn}} = \frac{\overline{P}^*_{\text{aero}}}{\overline{P}^*_{\text{aero}} + (\overline{P}^*_{\text{acc}} \cdot (1-\eta_{\text{elastic}}))} = \frac{\overline{P}^*_{\text{aero}}}{\overline{P}^*} \tag{12}$$

The values of η_{dyn} listed in Table 1 show that having longer wings help to maximise the aerodynamic contribution to the total power expenditure. This is because η_{dyn} increases with R but is constant for any value of n (based on eqns (4) and (12)). It is also evident that η_{dyn} will be extremely

Table 1: Values of dynamic efficiency, η_{dyn}, mean power, $\overline{P}$, and mean mass-specific power, $\overline{P}^*$, for 12 g MAVs A and B with 0%, 50% and 100% elastic storage, η_{elastic}.

	η_{elastic} (%)	η_{dyn} (%)	$\overline{P}^*$ (W/kg)	$\overline{P}$ (W)
MAV A	0	30.6	208.17	2.50
R = 75.0 mm, n = 33.6 Hz,	50	43.0	135.93	1.63
U_{max} = 8.8 m/s	100	100.0	63.70	0.76
MAV B	0	23.2	409.72	4.92
R = 50.2 mm, n = 75.0 Hz,	50	37.7	252.47	3.03
U_{max} = 13.1 m/s	100	100.0	95.23	1.14

poor for small-winged MAVs (e.g. 20 mm and below) unless significant elastic storage can be implemented. Of the two designs above, MAV A is superior to MAV B in many respects, unless the flight speed, U, is a critical parameter in the design. Table 1 lists the total mean power, $\overline{P}$, required by both 12 g MAVs. For MAV A, $\overline{P}$ ranges from 2.5 W for 0% elastic storage down to 0.76 W for 100% elastic storage, while for MAV B the power required is approximately double ranging from 4.92 to 1.14 W. However, it should be noted that the peak power requirement is likely to be around double these values.

In conclusion, for an MAV weighing 12 g, the power expenditure can be greatly reduced, if the wing length is maximised to 75 mm. Selecting shorter wings to increase the maximum flight speed was found to come at a high cost: the example presented above shows that to increase the flight speed by 50%, the power requirement approximately doubles.

4 ACTUATOR SELECTION

Actuator selection for a flapping MAV is challenging task, since the high power output requirement outlined in the previous section must be met within challenging dimensional, weight and energy source limitations. In particular, the actuator cannot be treated as a standalone device since the driver electronics, transmission mechanism and power supply all need to be included on-board the MAV to form the 'actuation system'. In general, actuators can be grouped into two main classes: rotary and linear. It is difficult to make isolated comparisons between each type of actuator, since the choice of actuator type fundamentally influences the complexity and performance of the associated flapping mechanism. At the miniature scale of MAVs, the optimum rotary devices are brushless DC motors as they currently have the highest power output per unit mass for high speed operation. However, it will be shown in Section 5 that a rotary input flapping mechanism is a non-optimal solution and the optimum actuator should have a linear output.

The stress-strain (scale-invariant force-stroke) performance of linear actuation technologies is as shown in Fig. 1. (A detailed evaluation of performance characteristics can be found in [21].) The ideal linear actuator should produce high power over a large stroke, so that inefficient amplification mechanisms can be avoided. Out of the commercially available actuators shown in Fig. 1, only shape memory alloy and solenoids have a comparable strain output as muscle and both are unsuitable due to low operational frequencies and energy density respectively. The strain output of piezoelectric ceramic actuators can be amplified via a bender configuration, but it is noticeable from Fig. 1 that the volume-specific energy per stroke is very low. The volume-specific *power* of piezoelectric ceramic actuators can be very large, but only at high frequency operation. Therefore, to generate enough power a high wingbeat frequency and short wing length are required, which from eqn (12) decreases dynamic efficiency.

Due to the performance limitations of commercially available actuation technologies, the application of the emerging class of electro-active polymers (EAPs) actuator should be considered for flapping MAVs. It can be seen in Fig. 1 that several types of EAP have a similar stress-strain output as muscle. It should be noted that the novel nature of EAP actuators means that certain fabrication or operational issues exist and are being gradually eradicated through research [22]. Despite this, the performance of dielectric elastomers closely matches that of an 'artificial muscle' and is thus highly desirable for implementation into a flapping MAV. The development of a dielectric elastomer actuator for flapping MAVs is presented in Section 6.

5 MAV FLAPPING MECHANISMS

The design of a fully optimised mechanism that produces a flapping output is critical to the flight performance of a flapping MAV. The flapping mechanism should transmit a rotary or linear input(s) into a combined flapping and pitching motion, which ideally should be dynamically adjustable to

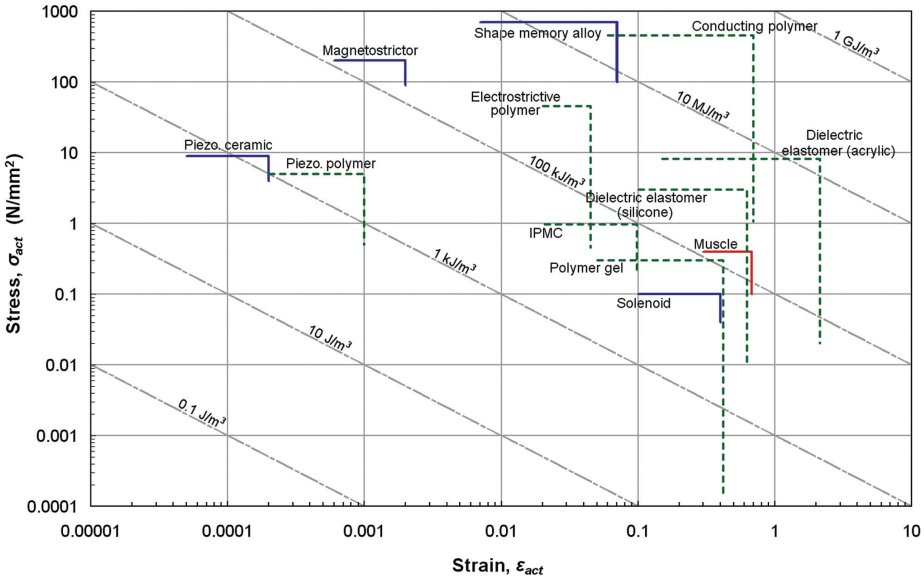

Figure 1: Maximum stress-strain performance limits for conventional actuators (*solid lines*), biological muscle and electro-active polymer actuators (*dashed lines*) (data from [21, 22]).

perform flight stability and manoeuvring (as outlined in Section 2). The flapping mechanism must also satisfy the general MAV criteria of being highly compact and lightweight. These limitations impose a great difficulty on the selection of a suitable mechanism. A survey of previously developed MAV flapping mechanisms by Conn *et al.* [15] has shown that only one design by Steltz *et al.* [23] produces a dynamically adjustable output. The remaining mechanisms are still feasible options for flapping MAVs, but must be combined with some non-biomimetic method of control, e.g. rudders and ailerons.

It is not coincidental that the only dynamically adjustable flapping mechanism surveyed in [15] has a linear input. For flapping MAVs, the level of constraint of the flapping mechanism is dependent on whether its inputs (i.e. actuators) are rotary or linear. Fundamentally, a linear input mechanism can be under-constrained since, generally, the magnitude of the output stroke of a linear actuator can be modulated to allow proportional control. High frequency operation dictates that the output stroke of rotary actuators cannot be proportionally modulated and prevents the use of antagonistic inputs, so the wing stroke amplitude can never be dynamically shortened or lengthened. This means a rotary input mechanism is more likely to have a constrained output where the wing trajectory is fixed to a single, highly repeatable path. It would appear, therefore, that selecting an under-constrained mechanism with a linear input is the direct solution. However, it was shown in Section 4 that there is a lack of linear output actuators that can produce the same high power over a large stroke output as biological muscle (this notion is validated by the fact the dynamically adjustable, linear input mechanism developed by Steltz *et al.* [23] utilises custom linear actuators). Two solutions to this combined issue of actuator performance limitations and mechanism constraint are presented here.

The first solution utilises a novel, rotary input mechanism called the parallel crank-rocker (PCR) that is *partially* constrained, i.e. one of its output degree of freedom (DoF) is dynamically adjustable. The PCR mechanism, which is shown schematically in Fig. 2a, comprises a pair of constrained

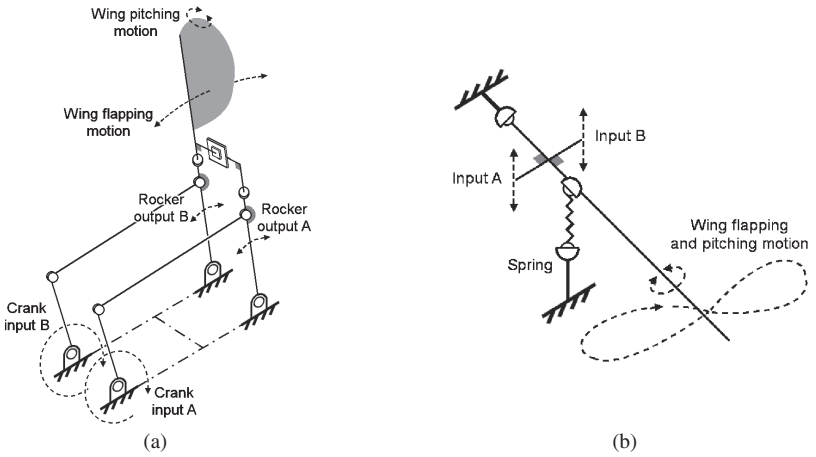

Figure 2: (a) Rotary input, partially constrained PCR mechanism; (b) linear input, under-constrained linkage.

1-DoF crank-rocker mechanisms that are coupled by an under-constrained 3-DoF coupling linkage. The result is a mechanism that has a fixed flapping motion and a dynamically adjustable pitching motion. This arrangement allows the wing angle of attack to be controlled, which is essential for both flight control and reproducing the unsteady aerodynamic phenomena discussed in Section 2. Control of the angle of attack is achievable by adjusting either the phase lag between the parallel cranks (inputs A and B in Fig. 2a) or the perpendicular distance between the rockers (outputs A and B in Fig. 2a). The link ratios of the PCR can be optimised so that wing kinematics closely match those of a typical insect [15]. The development of the PCR concept into a functional prototype flapping mechanism is described in Section 7.

The second solution to the issue of actuation limitations and mechanism constraint is the development of a mechanically simple, under-constrained mechanism of the basic configuration shown in Fig. 2b. The mechanism itself is effectively a 3-DoF first order lever that is well suited to resonant operation, as it could be fabricated using compliant hinges. The flapping motion is generated by modulating the linear inputs, which are applied either side of the wing fulcrum to affect wing pitching. The simple mechanism shown in Fig. 2b is only viable, if it is driven by high power actuators with a large stroke. Therefore, the key to this under-constrained solution is the development of an 'artificial muscle' actuator with these desired performance characteristics. The development of such an actuator, using the emergent technology of electro-active polymers, is described in Section 6.

6 DEVELOPMENT OF AN ARTIFICIAL MUSCLE ACTUATOR

6.1 Principle of operation

Dielectric elastomers are arguably the most promising 'artificial muscle' actuation material classed as electro-active polymers. Dielectric elastomer actuators operate on the electrostatic effect, where an elastomer film is placed between two compliant electrodes and when a voltage is applied the elastomer is squeezed in thickness and stretched in length and width. This response is caused by the

electrostatic forces generated between free charges on the electrode, where opposite charges on the two electrodes attract and like charges repel [22]. These electrostatic forces are proportional to the square of the applied electric field. Using a simple electrostatic model the pressure, p, exerted by the electrodes on a single elastomer film can be described with eqn (13) [24]:

$$p = e_r e_0 T^2 = e_r e_0 \left(V/h\right)^2 \tag{13}$$

where T is the applied electric field, V is the applied voltage, h is the elastomer film thickness, e_r is the relative dielectric constant of the elastomer and e_0 is the permittivity of free space (= 8.85×10^{-12} F/m). Assuming that the elastomer film is unloaded and unconstrained, the thickness strain, ε_z, is given by $-p/E$, where E is the Young's modulus of the elastomer. The planar strains ε_x and ε_y can be estimated from ε_y by using the generalised Hooke's law.

Although the principle behind dielectric elastomer actuators is relatively simple, there are several prominent features that need to be factored into the actuator design. In particular, a very strong electric field is required (typically 50–200 kV/mm). Advances in the miniaturisation of electronics mean that high voltages are feasible at MAV scales, but even the best performing micro step-up voltage converters are still limited to around 5–10 kV maximum output (e.g. EMCO Q50-5). Therefore the film thickness, h, must be very thin (~50 μm) for maximum performance. Also, the electrodes must be highly compliant, as it allows the like charges on either side of the dielectric layer to repel. In Section 5, the principle actuator performance criterion was defined as being mass-specific power. Benders are mass efficient strain amplifying mechanisms, which operate on the principle shown in Fig. 3. Benders allow multiple dielectric layers to be stacked up, which helps to maximise the power output while maintaining a large stroke. An important feature of bender actuators, in relation to flapping MAV design, is that the passive substrate provides elastic storage and hence reduces energy expenditure per stroke (when reciprocating). It is worth noting that a previous, aborted attempt by Zdunich *et al*. [25] to develop a dielectric elastomer-driven flapping MAV did not use the stacked bender configuration.

6.2 Fabrication of bender actuators

There are numerous different elastomers that can be utilised as dielectric actuators. A three-part TC-5005 silicone elastomer (BJB Enterprises Inc., USA) was selected, as it is suited to prototyping with a low cost and a third mixing component, a softening plasticizer, which allows the Young's modulus to be modified. The electrode material was fabricated by mixing 10 μm graphite carbon powder (Graphite Trading Company, UK) with uncured TC-5005 silicone. Three dielectric

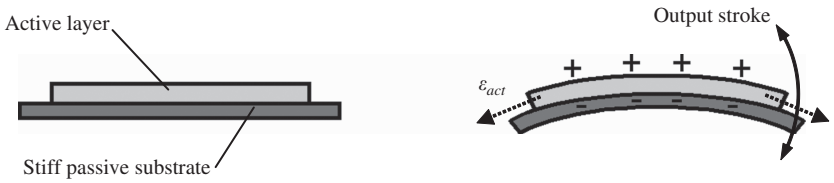

(a) *Inactive (voltage off)* (b) *Active (voltage on)*

Figure 3: Bender actuator principle: (a) inactive (voltage off); (b) active (voltage on). The planar output strain, ε_{act}, of the active layer causes the stiffer passive substrate to bend, producing an amplified output stroke.

elastomer bender actuators were produced for testing with 4, 8 and 12 active dielectric layers, respectively. Each bender had a 50.8 μm thick steel strip as the passive substrate with alternating layers of the active 500 μm thick dielectric elastomer and electrodes stacked on top. Due to the high voltages required for operation, an insulating layer of TC-5005 silicone was applied to each bender. The final 4-layer, 8-layer and 12-layer bender actuators used for testing weighed 4.15, 5.54 and 6.80 g, respectively, and had planform dimensions of 54 × 10 mm. During testing, the bender actuators were placed in a high voltage isolation box and were driven using an EMCO F12-TR voltage converter which outputs up to 12 kV.

6.3 Bender actuator performance

Measurements of the tip displacement for each bender actuator were taken using a digital camera fixed perpendicularly to the 2 mm grid, which allowed the relative motion from the inactive to active states to be quantified using image analysis software. The maximum output stroke produced by the 8-layer bender actuator occurred at the highest voltage supply before breakdown and is shown in Fig. 4. The 8-layer and 12-layer benders produced the greatest maximum tip displacements, δ_{tip}, of 18.2 and 20.2 mm, respectively. Using the tip displacement values, the theoretical blocking force of each actuator was estimated using the well-known cantilever stiffness equation [2]. This allowed estimates of work done per stroke, W_s, to be obtained. W_s was equal to 0.069 mJ for the 8-layer bender and 0.085 mJ for the 12-layer bender [2]. The 4-layer bender produced a maximum stroke of 9.1 mm and W_s equalled 0.017 mJ.

The tip displacements of the best performing 8-layer and 12-layer benders are equivalent to a bender-specific strain, ε_b, of 0.34 for the 8-layer bender and 0.37 for the 12-layer bender (where $\varepsilon_b = \delta_{tip}$/bender length). These values of ε_b are similar to the maximum strain output of a solenoid (~0.4) and are within the range of values associated with biological muscle (~0.3–0.7). The estimated work done per stroke, W_s, of 0.085 mJ for the 12-layer bender compares favourably to similarly sized commercial piezoelectric bender devices. Considering that the tested benders were preliminary designs and did not utilise the best performing elastomers available (e.g. 3M™ VHB 4910 or Dow Corning HSIII), these results strongly indicate that dielectric elastomer benders are suited for the high power output required for flapping MAVs. Although the bender actuators presented here require

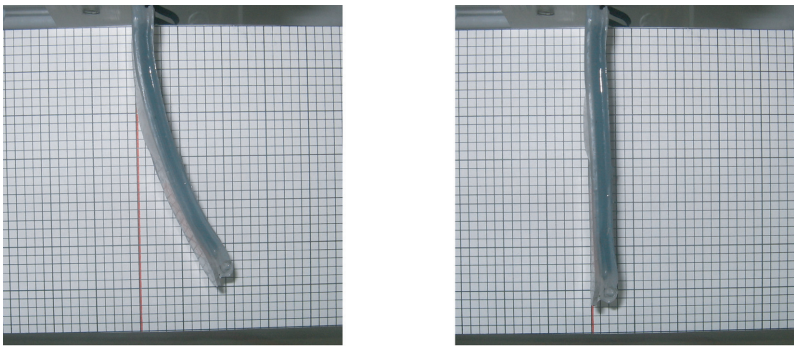

(a) Inactive (V = 0 kV) (b) Active (V = 6.8 kV)

Figure 4: The 8-layer dielectric elastomer bender actuators in its (a) inactive (V = 0 kV) and (b) active states (V = 6.8 kV) at the maximum applied voltage before dielectric breakdown.

further development and optimisation, these preliminary results have demonstrated the feasibility of producing under-constrained, kinematically adjustable flapping mechanisms, which will be capable of driving highly manoeuvrable flapping wing MAVs.

7 DEVELOPMENT AND TESTING OF AN MAV FLAPPING MECHANISM

7.1 Development of a PCR prototype

The concept for a novel rotary input mechanism called the PCR was presented in Section 5. The PCR design was developed into a functional prototype to act both as a proof of concept and as an experimental test-rig. Figure 5a shows a CAD view of the sub-assemblies that constitute the PCR prototype. The completed prototype is shown in Fig. 5b with 75 mm long wings constructed from carbon fibre wing spars and a Mylar™ wing membrane. A description of the design and fabrication of the PCR prototype is given in Conn *et al.* [15]. Excluding the wings, the complete assembly measured 25 × 29 × 62.75 mm with a total mass of 46 g. Three pairs of wings were fabricated for aerodynamic testing, which had the same basic construction with varying design parameters (camber and aspect ratio), as shown in Fig. 6. Two motors were used to drive the PCR prototype: the 0.75 W Maxon RE10 brushed DC motor and the 8 W Maxon EC10 brushless DC motor. The angle of attack produced by the PCR mechanism can be controlled via the phase lag between the parallel cranks. For the initial PCR prototype shown in Fig. 5, control of the crank phase lag was limited to manual adjustments, i.e. between operations. A second PCR prototype that includes the capacity to

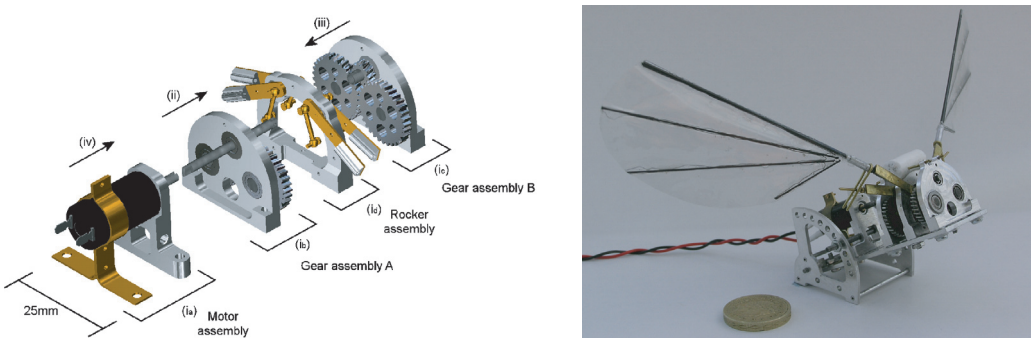

(a) (b)

Figure 5: (a) CAD assembly of the PCR mechanism with assembly order annotated; (b) fully assembled PCR prototype (shown with UK one pound coin for scale).

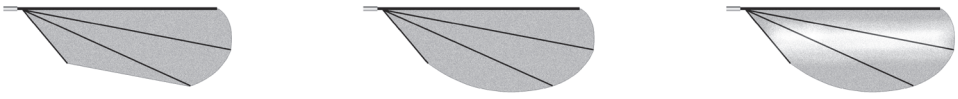

(a) Flat
$AR = 8.5$ $m = 0.43$ g

(b) Flat
$AR = 6.9$ $m = 0.44$ g

(c) Cambered
$AR = 6.9$ $m = 0.54$ g

Figure 6: Carbon fibre and Mylar™ wings with values of mass, m, and aspect ratio, AR: (a) flat, $m = 0.43$ g, $AR = 8.5$; (b) flat, $m = 0.44$ g, $AR = 6.9$; (c) cambered, $m = 0.54$ g, $AR = 6.9$.

dynamically adjust the angle of attack during operation is currently under development. It utilises a novel rotationally isolated pulley system that allows both PCR cranks to be driven by a single motor while the crank phase lag is adjusted using a separate servo motor.

7.2 Aerodynamic testing

The lift force produced by the PCR prototype in the hovering configuration (horizontal stroke plane and stagnant air) was measured. The lift measurement was carried out using a single-axis-Kyowa LTS-100GA load cell, with the PCR prototype mounted in line with the sensing axis so that the stroke plane was kept horizontal. A purpose-built strain gauge amplifier with signal conditioning was implemented in conjunction with the load cell and force measurements were recorded using a National Instruments NI-USB6211 data acquisition unit. A proximity sensor was aligned with one of the wings to synchronously measure stroke position along with the lift force. Each set of lift data was processed using a fourth order Butterworth low-pass filter with a 35 Hz cut-off frequency. Despite filtering the data, an inertial contribution to the force measurements caused by unwanted vibrations during stroke reversal could not be fully eliminated. As a result only the lift generated during the translatory phase of the wing stroke was used to generate values of mean lift, i.e. only during the downstroke and upstroke. The crank phase lag was kept constant during all tests so that the mid-stroke angle of attack remained constant at 40°.

Values of the mean translational lift force, $\overline{L}_t$, for the three wing types are shown in Fig. 7, where they are plotted against wingbeat frequency. Curves of predicted mean lift for various values of C_L

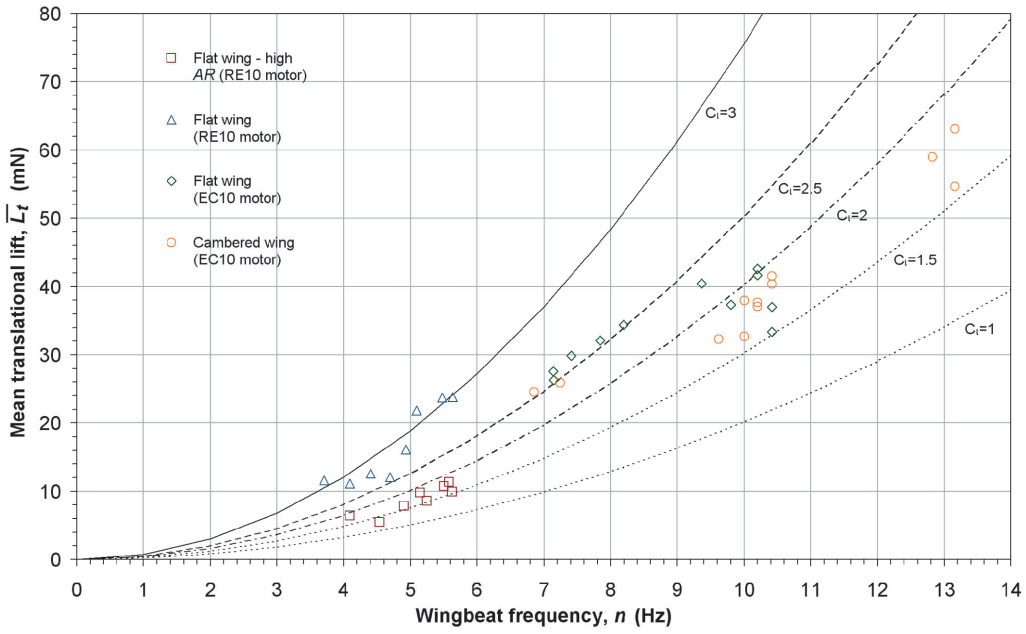

Figure 7: Measured mean translational lift for three wing pair types (flat with high *AR*, flat and cambered). Curves of predicted lift are given for various values of C_L, calculated using eqn (1).

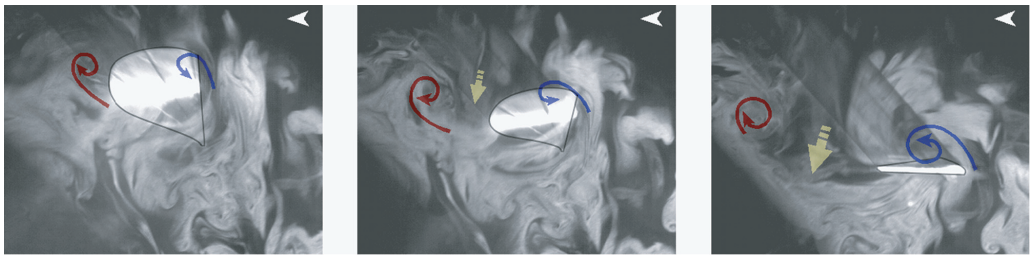

Figure 8: Vortex generation during downstroke (0.5 m/s air flow from right to left). (a) Starting vortices generated at both edges; (b) trailing edge vortex is shed while LEV is bound; (c) strong downwash (*dashed arrow*) observed in wing wake.

are included in Fig. 7, which were calculated using eqn (1) with $\Phi = 1.745$ rad, $R = 0.075$ m and $AR = 6.9$. From Fig. 7, it appears all three pairs of wings have a mean lift coefficient in the range of 1.5–2.5. The maximum value of $\overline{L}_t$ was measured as 63.1 mN (6.4 g) at 13.2 Hz for the cambered pair of wings. As expected, the low AR wings produced more lift than the high AR wings, although they undoubtedly generated more drag as well. It is notable from Fig. 7 that the flat and cambered wings with the same aspect ratio produced very similar values of lift. This implies that the extra lift produced on the cambered wing's downstroke negates any reduction on the upstroke. For the purpose of future wing designs, this result suggests that a wing with reversible camber (i.e. negative on both strokes) would be the optimum solution for hovering flight.

The unsteady nature of flapping wing aerodynamics means that flow visualisation is an important step towards evaluating the performance of the wing design and the kinematics produced by the PCR mechanism. Flow visualisation of the PCR mechanism was undertaken in a wind tunnel fitted with a polyethylene glycol-based particle seeder, a Photron Ultima APX high-speed camera and an Oxford Lasers LS 20-50 copper vapour laser. The laser light sheet was orientated perpendicular to the wing and was translated along the wing length in increments of 10 mm from base to tip during testing. The wing tunnel flow velocity was maintained at 0.5 m/s throughout testing.

Flow separation at both the leading and trailing wing edges was found to occur within the first 15–20° of the stroke with vortices forming immediately after. The timing of LEV generation found here appears to be similar to a study of hawkmoth aerodynamics, where a clear LEV was observed 21° into the stroke [26]. The trailing edge vortex was shed shortly after this point in the presence of a strong downwash flow, as shown in Fig. 8. The downwash remained in the wake throughout the downstroke and flowed between the initially shed trailing edge vortex and the bound LEV. Comparisons between footage taken with the laser sheet in different positions along the wing suggested the presence of a connected vortex wake. There were also qualitative indications that the presence of the LEV and shed trailing edge vortex increased the downwash velocity. The presence of a stable, bound LEV on the downstroke suggests that the PCR mechanism and selected angle of attack generates enhanced lift through at least one unsteady aerodynamic mechanism (delayed stall).

8 CONCLUSION

The design and optimisation of a flapping wing MAV that aims to replicate the highly agile flight of insects is a challenging task, which has not yet been met. A study of the power expenditure required to support a 12 g flapping MAV during hover was undertaken. The results of this study showed that the actuated flapping mechanism within the 12 g MAV has to deliver between 1.5 and 5 W of

mechanical power, depending on certain design parameters. In particular, the trade-off between wing length and wingbeat frequency is critical, where having shorter wings and a higher wingbeat frequency increases flight speed at the cost of increased power expenditure. For the design parameters selected, a 50% increase in flight speed through wing length reduction required 100% more power.

For agile and manoeuvrable flight comparable to that of insects, it is crucial that the MAV flapping mechanism produces a dynamically adjustable output so that the wing kinematics (i.e. angle of attack, stroke amplitude and timing) are controllable. An under-constrained mechanism is well suited for this type of kinematic adjustability. However, to develop such a mechanism at MAV scale requires an 'artificial muscle' actuator that can deliver high power over a large stroke. Since actuators that meet this requirement are not currently available, a majority of previously developed flapping mechanisms have been driven by rotary DC motors, and as a result, are fully constrained with no kinematic adjustability. Two solutions to this combined issue of actuator performance limitations and mechanism constraint were presented.

The first solution is the development of an 'artificial muscle' using silicone dielectric elastomer films. This emergent class of actuator has been developed into several prototypes, which were configured as stacked benders to maximise power output and to incorporate embedded elastic storage (which was shown to be extremely important in study of power requirements). The preliminary results showed a maximum strain output of 0.37, which is within the range of values associated with biological muscle (~0.3–0.7). However, the work done per stroke needs to be increased, which should be achievable by minimising the current elastomer film thickness from 500 μm to under 100 μm.

The second solution has been the development of a novel partially constrained mechanism called the PCR, which allows dynamic adjustability of the wing angle of attack despite being driven by a rotary DC motor. A PCR prototype that is optimised to reproduce the wing kinematics of insects was developed and aerodynamically tested. Lift measurements of the PCR prototype suggested that the tested wing designs have a mean lift coefficient in the range of 1.5–2.5. The maximum lift force of 6.4 g at a wingbeat frequency of 13.2 Hz will need to be increased in future designs, most probably through the use of a higher power brushless DC motor and the optimised implementation of elastic storage. High-speed footage of flow visualisation tests in a wind tunnel confirmed the existence of at least one of the lift enhancing unsteady aerodynamic mechanisms exploited by insects: the leading edge vortex with delayed stall.

Designing and fabricating an actuated flapping mechanism that combines a high power output with dynamically adjustable wing kinematics is critical to the success of an insect-inspired flapping MAV. The two designs presented here that overcome issues of actuation limitations and mechanism constraint both require further optimisation, but offer viable solutions to one of the most challenging aspects of flapping MAV design.

ACKNOWLEDGMENTS

This work is supported by the UK Engineering and Physical Science Research Council (EPSRC) under grant number EP/C535286/1. The authors also wish to thank the EPSRC Engineering Instrument Pool for loaning the high-speed camera and Particle Image Velocimetry system and to Dantec Dynamics Ltd. for loaning the particle seeding generator.

REFERENCES

[1] Muller, T.J. & DeLaurier, J.D., An overview of micro air vehicle aerodynamics (Chapter 1). *Fixed and Flapping Wing Aerodynamics for Micro Air Vehicle Applications – Progress in Astronautics and Aeronautics Volume 195*, American Institute of Aeronautics and Astronautics: Virginia, USA, pp. 1–10, 2001.

[2] Conn, A.T., *Development of novel flapping mechanism technologies for insect-inspired micro air vehicles*. PhD Thesis, University of Bristol, 2008.
[3] Aubépart, F. & Franceschini, N., Bio-inspired optic flow sensors based on FPGA: application to micro-air-vehicles. *Microprocessors and Microsystems*, **31**, pp. 408–419, 2007.
[4] Skordos, A.A., Chan, P.H., Vincent, J.F. & Jeronimidis, G., A novel strain sensor based on the campaniform sensillum of insects. *Philosophical Transactions of the Royal Society A – Mathematical Physical and Engineering Sciences*, **360**, pp. 239–253, 2002.
[5] Jones, K.D. & Platzer, M.F., Bio-inspired design of flapping wing micro air vehicles – an engineer's perspective. *44th Aerospace Sciences Meeting and Exhibit*, Reno, NV, 9–12 January 2002.
[6] Lentink, D., Bradshaw, N.L. & Jongerius, S.R., Novel micro aircraft inspired by insect flight. *Comparative Biochemistry and Physiology Part A*, **146A**, Supplement 1 (April 2007), pp. S133–S134, 2007.
[7] Pornsin-Sirirak, N., Tai, Y.C., Ho, C.M. & Keenon, M., Microbat – a palm-sized electrically powered ornithopter. *NASA/JPL Workshop on Biomorphic Robotics*, Pasadena, CA, 14–17 August, 2001.
[8] Ellington, C.P., van den Berg, C., Willmott, A.P. & Thomas, A.L.R., Leading-edge vortices in insect flight. *Nature*, **384**, pp. 626–630, 1996.
[9] Dickinson, M.H., Lehmann, F.-O. & Sane, S.P., Wing rotation and the aerodynamic basis of insect flight. *Science*, **284**, pp. 1954–1960, 1999.
[10] Birch, J.M. & Dickinson, M.H., The influence of wing–wake interactions on the production of aerodynamic forces in flapping flight. *Journal of Experimental Biology*, **206**, pp. 2257–2272, 2003.
[11] Weis-Fogh, T., Quick estimates of flight fitness in hovering animals, including novel mechanisms for lift production. *Journal of Experimental Biology*, **59**, pp. 169–230, 1973.
[12] Sane, S.P. The aerodynamics of insect flight. *Journal of Experimental Biology*, **206**, pp. 4191–4208, 2003.
[13] Lehmann, F.-O., The mechanisms of lift enhancement in insect flight. *Naturwissenschaften*, **91**, pp. 101–122, 2004.
[14] Michelson, R.C., Novel approaches to miniature flight platforms. *Proceedings of the Institution of Mechanical Engineers, Part G: Journal of Aerospace Engineering*, **218**, pp. 363–373, 2004.
[15] Conn, A.T., Burgess, S.C. & Ling, C.S., Design of a parallel crank-rocker flapping mechanism for insect-inspired micro air vehicles. *Proceedings of the Institution of Mechanical Engineers, Part C: Journal of Mechanical Engineering Science*, **221**, pp. 1211–1222, 2007.
[16] Taylor, G.K. Mechanics and aerodynamics of insect flight control. *Biological Reviews of the Cambridge Philosophical Society*, **76**, pp. 449–471, 2001.
[17] Ellington, C.P. The novel aerodynamics of insect flight: applications to micro-air vehicles. *Journal of Experimental Biology*, **202**, pp. 3439–3448, 1999.
[18] Ellington, C.P., The aerodynamics of hovering insect flight. III. Kinematics. *Philosophical Transactions of the Royal Society of London Series B*, **305**, pp. 41–78, 1984.
[19] Dudley, R., *The Biomechanics of Insect Flight: Form, Function, Evolution*, Princeton University Press: Princeton, NJ, pp. 148–149, 2000.
[20] Ellington, C.P., The aerodynamics of hovering insect flight. VI. Lift and power requirements. *Philosophical Transactions of the Royal Society of London Series B*, **305**, pp. 145–181, 1984.
[21] Huber, J.E., Fleck, N.A. & Ashby, M.F., The selection of mechanical actuators based on performance indices. *Proceedings of the Royal Society of London A*, **453**, pp. 2185–2205, 1997.

[22] Bar-Cohen, Y., *Electroactive Polymer (EAP) Actuators as Artificial Muscles – Reality, Potential and Challenges*, 2nd edn, SPIE Press: Bellingham, WA, 2004.
[23] Steltz, E., Avadhanula, S. & Fearing, R.S., High lift force with 275 Hz wing beat in MFI. *IEEE International Conference on Intelligent Robots and Systems*, San Diego, 29 October–2 November 2007.
[24] Pelrine, R., Kornbluh, R. & Joseph, J., Electrostriction of polymer dielectrics with compliant electrodes as a means of actuation. *Sensors and Actuators A: Physical*, **64**, pp. 77–85, 1998.
[25] Zdunich, P., Bilyk, D., MacMaster, M., Loewen, D., DeLaurier, J., Kornbluh, R., Low, T., Stanford, S. & Holeman, D., Development and testing of the Mentor flapping-wing micro air vehicle. *Journal of Aircraft*, **44**, pp. 1701–1711, 2007.
[26] van den Berg, C. & Ellington, C.P., The vortex wake of a 'hovering' model hawkmoth. *Philosophical Transactions of the Royal Society of London Series B*, **352**, pp. 317–328, 1997.